Monthly Notices
of the
ROYAL ASTRONOMICAL SOCIETY

MNRAS **490,** 2254–2261 (2019)
Advance Access publication 2019 September 21

doi:10.1093/mnras/stz2655

Heavy negative ion growth in Titan's polar winter

A. Wellbrock,[1,2]★ A. J. Coates,[1,2]★ G. H. Jones,[1,2] V. Vuitton,[3] P. Lavvas,[4] R. T. Desai[5] and J. H. Waite[6]

[1]*Mullard Space Science Laboratory, University College London, Dorking RH5 6NT, UK*
[2]*The Centre for Planetary Sciences at UCL/Birkbeck, London WC1E 6BT, UK*
[3]*Chargée de recherche au CNRS, Institut de Planétologie et d'Astrophysique de Grenoble, Grenoble 38000, France*
[4]*Groupe de Spectrométrie Moléculaire et Atmosphérique (GSMA), UMR CNRS 7331, Université de Reims, Reims 51687, France*
[5]*Blackett Laboratory, Imperial College London, London SW7 2AZ, UK*
[6]*Southwest Research Institute, San Antonio, Texas 78238, USA*

Accepted 2019 September 11. Received 2019 August 6; in original form 2019 June 6

ABSTRACT

A significant but unexpected result of the Cassini mission was the discovery of heavy organic negative ions in Titan's ionosphere at altitudes between about 950 and 1400 km by the CAPS Electron Spectrometer (ELS). The heaviest ions were observed during the T16 fly-by with masses over 13 000 u/q. This is significantly higher than the maximum masses observed during other fly-bys. We study T16 CAPS-ELS observations and examine the evolution of mass spectra at different altitudes. We also study maximum mass trends using a large data set from all available CAPS-ELS observations of the Cassini mission in order to investigate the conditions necessary to allow negative ions to grow to the highest masses. For the first time, we are able to investigate the relationship between the highest mass particles and seasonal effects. We find that the combination of high latitude and winter conditions, resulting in long-term restricted solar flux, create an environment in which ion growth can reach the highest masses, as observed during T16. Restricting solar flux long term, and hence photodestruction reactions such as photodetachment, appears to be essential for negative ions to grow beyond 10 000 u/q.

Key words: astrochemistry – planets and satellites: atmospheres – planets and satellites: individual: Titan.

1 INTRODUCTION

Titan orbits Saturn at a distance of $20R_S$ (where $1R_S$ is Saturn's radius, 60 268 km) and is the second largest moon in our Solar system with a radius of 2576 km (Waite et al. 2005; Hörst 2017; Nixon et al. 2018). It has a very dense and extended nitrogen and methane-based atmosphere with an exobase at around 1500 km (Cui, Yelle & Volk 2008). Titan does not possess a significant intrinsic magnetic field (Backes et al. 2005; Wei et al. 2010). Therefore, being located in Saturn's outer magnetosphere under typical solar wind dynamic pressures, Titan's atmosphere interacts directly with Saturn's magnetospheric plasma (Brown, Lebreton & Waite 2010) in a similar fashion to the interaction of Mars, Venus, and comets with the solar wind, where the external plasma's magnetic field lines drape around the unmagnetized object. Titan's axial tilt of 26.7° is the same as Saturn's; therefore, the two bodies experience the same seasons where one year lasts 29.46 Earth years.

Negative ions at Titan were first detected by Cassini's CAPS Electron Spectrometer (ELS) during the first Titan fly-bys (Coates et al. 2007; Waite et al. 2007). They have subsequently been observed by CAPS-ELS in every sampled part of Titan's ionosphere, provided the altitude was below approximately 1400 km and CAPS pointed in the ram direction (see also Section 3 for a more detailed description). They therefore appear to be a permanent (yet variable) feature of Titan's highly complex ionosphere. Due to the presence of methane in Titan's atmosphere, the negative ion species present are mostly organic and range from low mass ions such as CN^- (product of e.g. electron attachment reactions) (Ali et al. 2015; Vuitton et al. 2009, 2019; Desai et al. 2017b; Mukundan & Bhardwaj 2018) to long carbon chain ions with masses exceeding 10 000 u/q (Coates et al. 2009; Michael et al. 2011; Lavvas et al. 2013; Lindgren et al. 2017). The highest masses are observed at the lowest sampled altitudes (950 km) (Coates et al. 2009, 2010a). Anion growth in Titan's ionosphere has also been studied in laboratory experiments (e.g. Dubois et al. 2019 and references therein). Densities are observed to peak at a range of altitudes depending on mass; the heaviest densities tend to peak near 1000 km whereas lighter ion

★ E-mail: a.wellbrock@ucl.ac.uk (AW); a.coates@ucl.ac.uk (AJC)

densities reach a peak around 1050 km (Wellbrock et al. 2013). The presence of these negative ions has also been confirmed by Cassini RPWS measurements (Ågren, Edberg & Wahlund 2012).

Low-mass negative ions have been observed in several planetary environments, e.g. the ionospheric D region at Earth (and references therein Hargreaves 1992), in the inner coma of comets 1P/Halley (Chaizy et al. 1991), and at Saturn's moons Rhea (Teolis et al. 2010; Desai et al. 2018), Dione (Nordheim et al. in preparation), and Europa (Volwerk, Kivelson & Khurana 2004; Desai et al. 2017a). In addition, negative water group cluster ions (Coates et al. 2010b) and negatively (as well as positively) charged nanograins (e.g. Jones et al. 2009) have been detected in Enceladus' plumes which are of comparable masses to the negative ions discussed here. Negatively charged carbon chain ions have also been observed in the interstellar medium (and references therein Cordiner et al. 2013; Millar, Walsh & Field 2017). Heavy organic anions can be found in other atmospheres where photochemical reactions involving nitrogen and methane are present, e.g. at Triton (Broadfoot et al. 1989), Pluto (Gladstone et al. 2016), and Charon (Grundy et al. 2016), where New Horizons data have shown that tholins may be responsible for red colouration. Therefore, heavy organic anion chemistry may be common in many different astrophysical environments, including extrasolar planets and moons.

The lowest Titan fly-bys by Cassini when CAPS was pointed in the ram direction were 950 km above Titan's surface, though the presence of negative ions below 900 km was confirmed using Cassini-RPWS data (Ågren et al. 2012). Shebanits et al. (2013) and Shebanits et al. (2016) showed that the negative charge density in Titan's deep ionosphere is dominated by negative ions and hence exhibits dusty plasma characteristics. The CAPS instrument was turned off during 2011 June–2012 March and then permanently after 2012 June. CAPS-ELS is uniquely capable of measuring the mass spectrum of negative ions and has observed them during more than 35 Titan fly-bys, the most recent one being T83 on 2012 May 22. CAPS-ELS measurements of negative ions allow the study of (i) negative ion mass, e.g. when and where in the ionosphere do we find the highest masses, and (ii) the amount present in different parts of the ionosphere (i.e. number density); this includes densities for different mass groups (see e.g. Wellbrock et al. 2013, Section 4). The former was investigated by Coates et al. (2009) who used CAPS-ELS data up to T48 (2008 December 5). With a larger data set available, this study investigates where the highest masses are found from a long-term perspective, allowing us to look for seasonal trends for the first time. The growth mechanisms of negative ions at Titan are still poorly understood, especially paths that lead to masses of 10 000 amu q^{-1} and above. We hope that by identifying and studying the conditions in which these ions can grow to such high masses, the results will allow future modelling and laboratory studies to improve our understanding of these highly complex processes. A complete list of all fly-bys studied here is available in the Appendix. The T16 fly-by, where the highest negative ion masses at Titan were detected, took place on 2006 July 22 (between the 2002 northern winter solstice and the 2009 equinox) at 00:25 UTC with a closest approach (CA) altitude of 950 km, a solar zenith angle (SZA) of 107° and a latitude of 85°N.

2 DATA ANALYSIS

CAPS-ELS is a top-hat electrostatic analyser (ESA), and one of the three sensors that make up the CAPS suite (Young et al. 2004). CAPS-ELS is capable of analysing negatively charged particles with an energy per charge between 0.5 eV and 26 keV. The

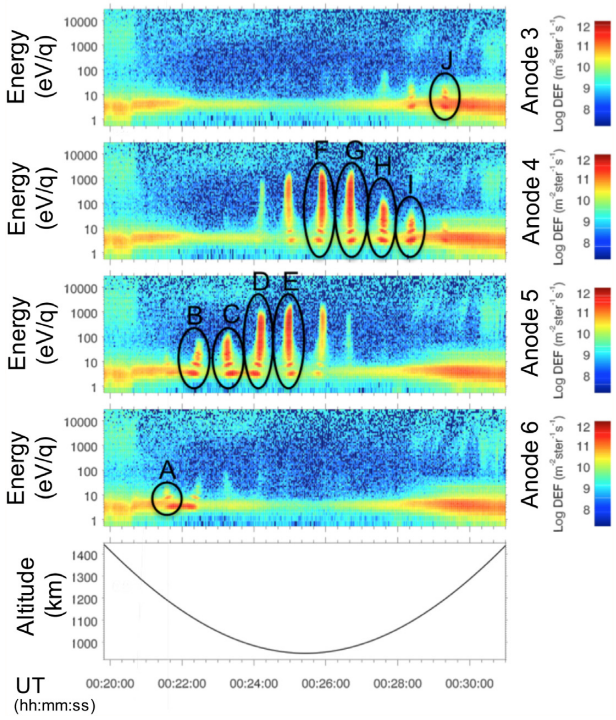

Figure 1. Cassini CAPS Electron Spectrometer (ELS) data from the Titan T16 fly-by. Top 4 panels: Spectrograms from anodes 3–6. The colour scale shows differential energy flux (DEF). Negative ion signatures are marked by black ellipses and labelled A–J. The vertical axis shows energy per charge which can be converted to mass per charge for the negative ions (see Section 3). Bottom panel: Altitude above Titan's surface in km. The horizontal axis shows universal time (UT) in hh:mm:ss.

energy resolution is 16.7 per cent and the energy bins are spaced logarithmically to match this intrinsic resolution, i.e. energy bins at higher energy cover larger energy ranges. Eight anodes, or instrument sectors, provide directional information and each has an angular coverage of 20° × 5°. To increase the field of view, the instrument is mounted on a rotating platform, or actuator, which can rotate at a nominal rate of 1° s^{-1} through a maximum range of ±104°.

Fig. 1 shows T16 spectrograms from anodes 3–6 and fly-by altitude information in the bottom panel. The circled spike-shaped structures labelled A–J in the spectrograms represent negative ion measurements and we refer to each structure as a negative ion signature. CAPS-ELS was actuating through a range of ±11° during this fly-by, centred around the ram direction i.e. the direction in which the spacecraft is travelling. The instrument only detects negative ions when it points in or very near the ram direction. We see spike-shaped structures in the spectrogram rather than continuous measurements of negative ions because the instrument does not point in the ram direction continuously but is actuating. Therefore, the spike-shaped structures appear when the instrument points in the ram direction, and the gaps appear when the instrument continues its actuation cycle i.e. when it points away from the ram direction temporarily, until it reverses direction and comes back to the ram direction to observe another spike-shaped negative ion structure, and so on.

The spacecraft was also rotating during T16 which is why negative ions are seen in different anodes. During signature *A*, anode 6 pointed in the ram direction and the strongest negative ion signal

was measured by this anode, whereas e.g. anode 3 did not observe any negative ion signal at this time due to pointing in a very different direction. Half an actuator cycle later anode 5 pointed in the ram direction due to the spacecraft's rotation, and hence detected the strongest negative ion signal at this time (signature *B*). A short while later (after further spacecraft rotation), anode 4 and then anode 3 pointed in the ram direction and detected the strongest signals. The neighbouring anodes show traces of negative ions in some cases, as they still pointed in a direction close to ram.

Negative ions are only observed when the instrument points in the ram direction for the following reason. In the Titan frame, the negative ions are very slow compared to the spacecraft. The ions are cold and hence only enter the instrument when they are rammed into; electrons on the other hand are observed in any direction due to their higher thermal velocities and relatively isotropic distributions (Coates et al. 2007, 2009, 2010a; Wellbrock et al. 2013; Desai et al. 2017b).

By assuming the observed ram energy is the kinetic energy of the ions and the spacecraft velocity is the relative speed, we can therefore determine the negative ion mass per charge, given by $m/q = 2qE/v^2$, where E is the observed (spacecraft potential corrected) energy per charge and v is the spacecraft velocity. Converting mass and energy units to u/q and eV, respectively, $m_{\mathrm{u/q}} = cE_{\mathrm{eV}}$, where c is the conversion factor $c = 1.93 \times 10^8/v^2$. As an example the spacecraft velocity during T16 at CA was 5.97 km s^{-1}, so c at this time is 5.42. As we are using an ESA, measurements are in energy per charge therefore we cannot determine q separately. We therefore present mass data in units mass per charge. Ions carrying multiple charges would have higher masses. This conversion implies that in the spectrogram, the spike-shaped structures represent negative ion mass distributions: The lowest masses are at the bottom, and the highest masses at the top. The observed energy E above is corrected for spacecraft potential as measured by Cassini's Radio and Plasma Wave Science (RPWS) Langmuir Probe (LP; Gurnett et al. 2004).

To obtain a 'pure' or processed negative ion count rate, we need to subtract the electron background. This can be done by choosing an anode that does not point in the ram direction. For example, in Fig. 1, anode 6 is used to measure the negative ion count rate for signature *A*. In this case, anodes 3 or 4 can be used to get a sample of the electron background at the same time as the negative ion time stamp, because no negative ions are detected in these anodes at the time when signature *A* is observed. To ensure the count rates are consistent, an inter-anode normalization is applied. This introduces a source of random uncertainty. In addition, even though electron distributions are generally isotropic in this environment, the fact that the electron background anode points in a different direction to the negative ion anode introduces another source of random uncertainty (also see Wellbrock et al. 2013).

3 RESULTS

Fig. 2 shows mass spectra of each negative ion signature observed during T16. The labels A–J correspond to the signature labels shown in Fig. 1. The unit 'counts per second' is an instrument specific unit. The width of the rectangles represents the range of the energy (i.e. mass) bins, which is equal to the intrinsic energy resolution of 16.7 per cent. As we are measuring a flux in the ram direction only, counts s^{-1} is proportional to number density (see Coates et al. 2007; Wellbrock et al. 2013), but note that the instrument energy bins are spaced logarithmically. This means that higher mass bins cover a larger range of masses, and hence the count rate (and density) is likely to be higher too.

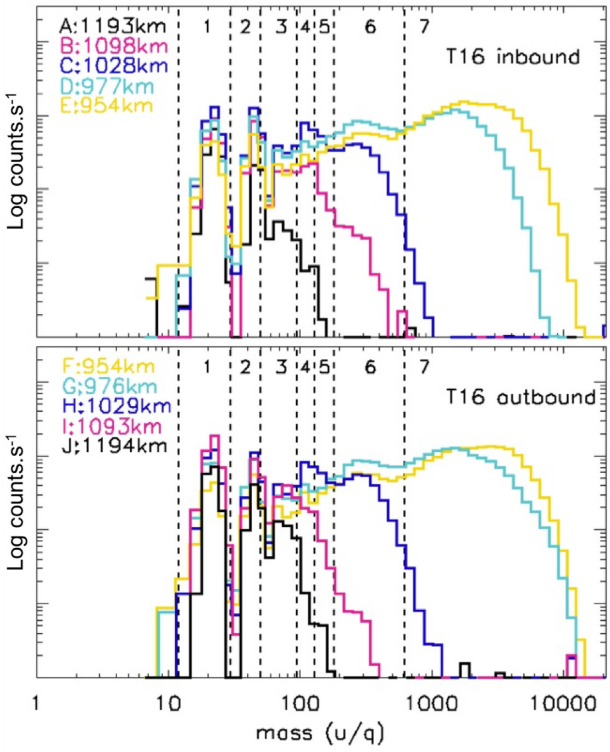

Figure 2. T16 negative ion mass spectra from CAPS-ELS. Top panel: Inbound data. Bottom panel: Outbound data. The different colours correspond to the labels A–J which also mark the matching negative ion signature in Fig. 1. The vertical dashed lines mark the boundaries of the different negative ion mass groups (see Section 3).

CAPS-ELS is not a mass spectrometer and was designed and calibrated to measure electrons, not negative ions. However, Coates et al. (2007) introduced a number of mass groups based on recurring peaks in the mass spectra observed during the early Titan fly-bys, which were updated by Wellbrock et al. (2013): group 1: 12–30 u/q; group 2: 30–55 u/q; group 3: 55–95 u/q; group 4: 95–130 u/q; group 5: 130–190 u/q; group 6: 190–625 u/q; group 7: 625 u/q and above. For a large part of the mass range observed, the energy (and hence mass) resolution of the instrument does not allow the identification of individual species. We can, however, study the behaviour of these groups of masses, which are likely to contain a number of different species, especially at higher mass due to the larger mass bins. The boundaries of the mass groups are marked by vertical dashed lines in Fig. 2 and the mass group numbers are shown between these. Vuitton et al. (2009) used a chemical model to identify mass groups 1–3 as CN^-, C_3N^-, and C_5N^-, respectively, with C_4H^- also contributing to mass group 3 at altitudes above 1100 km. Desai et al. (2017b) used a forward model of the CAPS-ELS response function to statistically identify these molecules and increase the mass resolution for mass groups 1–3, making it possible to differentiate between some species within these groups. Dobrijevic et al. (2016) and Mukundan & Bhardwaj (2018) also developed photochemical models of the lower mass chemistry.

The mass spectra (Fig. 2) show the evolution of the different mass groups at different altitudes. At higher altitudes, only the lower mass groups are present. As altitude decreases, higher mass groups start to develop, and the highest masses are present at the lowest altitudes (cf. Coates et al. 2009 and Figs 3a and b).

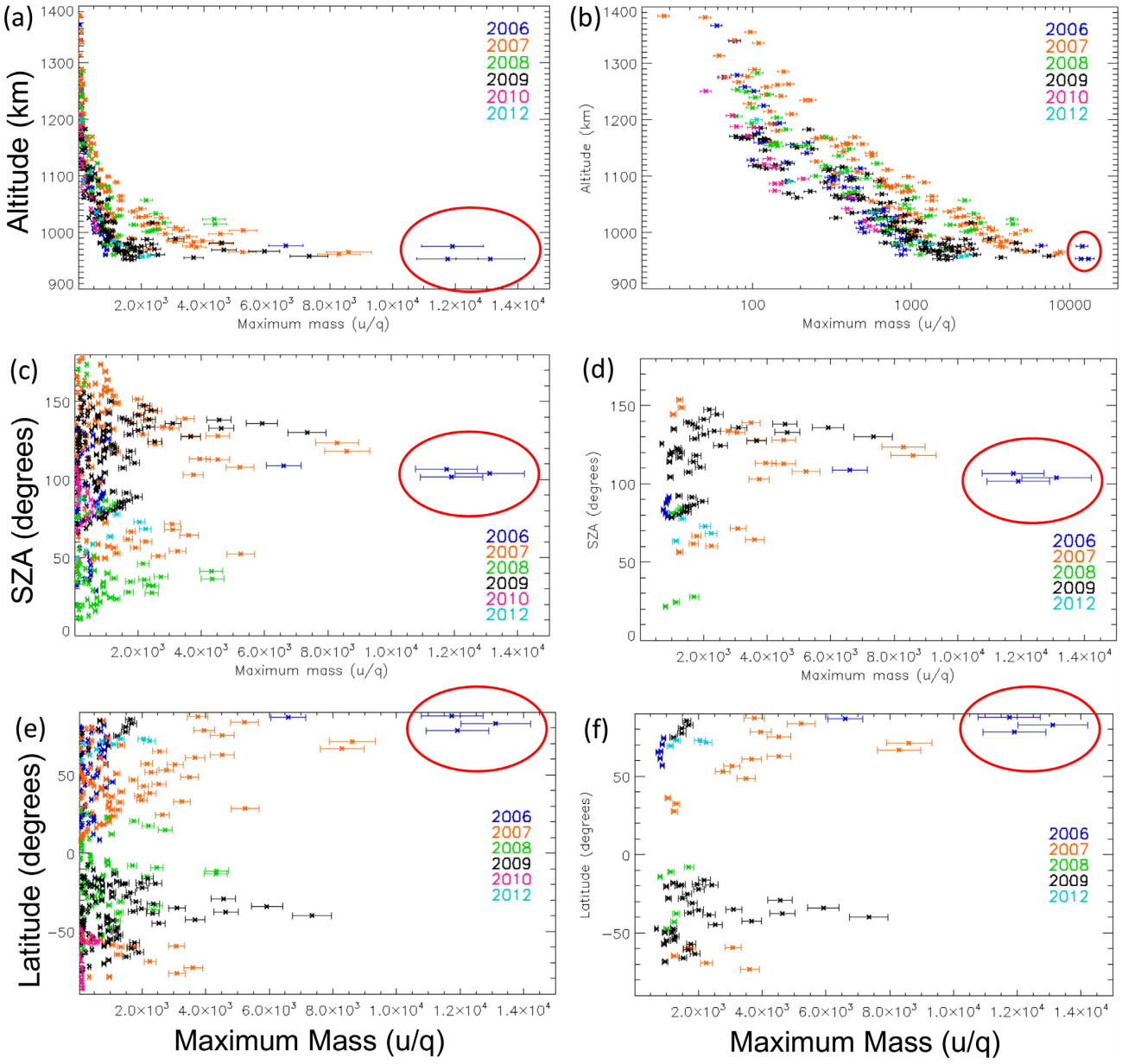

Figure 3. Maximum negative ion mass data plots. Each data point is the maximum mass recorded during individual negative ion signatures such as T16 signatures A–J in Fig. 1. The data points are from all negative ion fly-bys where CAPS-ELS detected negative ions and pointing conditions were favourable (see the Appendix for a complete list of fly-by and ephemeris data). The colours indicate the year of the fly-by. These plots are a continuation of Coates et al. (2009). The data points marked by the red circle are the maximum masses from T16 signatures *E*, *F*, and *G* (see Figs 1 and 2). Panels (a) and (b) show altitude above Titan's surface on a linear (a) and logarithmic (b) scale. Panels (c) and (e) show Titan SZA and latitude, respectively. Panels (d) and (f) are the same as (c) and (e), respectively, but show data observed at altitudes <1000 km only.

We note that only ten negative ion data points were measured during this fly-by which also happen to be almost perfectly symmetric about CA in terms of altitude, e.g. the first and the last data points are at 1193 and 1194 km, respectively, and the two points closest to CA are both at 954 km. We therefore only really sample approximately five different narrow altitude ranges, at slightly different locations in Titan's ionosphere. The corresponding inbound and outbound spectra at approximately the same altitude are shown in the same colour (e.g. *C* and *H* are in blue).

Coates et al. (2009) examined trends of maximum negative ion mass with altitude, Titan latitude and SZA using CAPS-ELS data from Titan fly-bys up to T48 (2008 December 5). We extend this study by including all negative ion observations detected by CAPS-ELS, where pointing conditions are favourable (see the Appendix), which allows us to also consider seasonal and longer-term controlling factors. The results are shown in Fig. 3. One data point corresponds to one negative ion signature such as the examples circled in Fig. 1. The data points show the maximum recorded mass during that signature. The spike-shaped circled signatures in Fig. 1 represent a mass distribution; hence, the lowest masses are at the bottom of the structure, and the highest masses at the top. Therefore, the maximum mass of each signature is taken from the very top of the signature. There are approximately ten signatures per fly-by. The 34 fly-bys examined here make up a total of 339 data points. The error

Table 1. Polar fly-bys during the Cassini mission where negative ions were detected with CAPS-ELS. In this study, we refer to a polar fly-by as having a CA latitude ≥80°.

Fly-by	Date	CA altitude (km)	CA SZA	CA latitude	Maximum mass (u/q)
T16	2006 July	954	107°	85°N	13 400
T32	2007 June	965	103°	87°N	5600
T64	2009 Dec	952	87°	83°N	1700
T65	2010 Jan	1074	96°	82°S	200

bars on the plot take into account several sources of uncertainty. This includes uncertainties that affect the count rate such as the electron background subtraction, inter-anode scaling, and spacecraft potential. The count rate is used to determine exactly what the maximum mass (i.e. the 'top' of the signature) is. The dominant uncertainty in the maximum mass determination is, however, the energy resolution of the instrument, which is 16.7 per cent.

The mass-altitude dependence Figs 3(a) and (b) show clearly that the highest masses are observed at the lowest sampled altitudes, as discussed in more detail by Coates et al. (2009). In addition, there is a group of data points made up of mostly orange (2007) and green (2008) observations that are higher in mass than the average at a specific altitude.

The mass-SZA dependence Fig. 3(c) shows a range of masses on both the day and night side; the very highest masses are observed on the night side at 105° to 140° SZA.

The mass-latitude dependence Figs 3(e) and (f) show that the very highest masses are found in the polar regions; however, there are also some medium to high masses at mid-latitudes. The three highest data points (marked by a red circle in all Fig. 3 panels) are the maximum masses recorded from T16 signatures *E*, *F,* and *G* in Figs 1 and 2. Four of the 34 fly-bys where negative ions were observed by CAPS-ELS were polar fly-bys. In this study, we refer to polar fly-bys as fly-bys where CA took place at a latitude ≥80°N or S. These fly-bys are shown in Table 1 and in the Appendix. The maximum masses observed during these polar fly-bys decrease as we move away in time from 2006.

We note that a large number of the low-mass data points in Figs 3(c) and (e) are low simply because of the altitude bias demonstrated in Figs 3(a) and (b). Heavier ions are only present at lower altitudes, whereas lighter ions are present at a wider range of altitudes. To demonstrate this effect and also to give an indication of the sampling, Figs 3(d) and (f) show the SZA and latitude dependence again but for data points observed in the altitude range of 950–1000 km only (950 km being the lowest sampled altitude). Therefore, these plots do not show data points that may only be low in mass because they were observed at higher altitudes and hence subject to the altitude bias.

4 DISCUSSION

The formation of negative ions in Titan's ionosphere starts with the photodissociation of the main atmospheric constituents, methane and nitrogen. Chemical reactions such as electron attachment produce a large variety of lower mass carbon and nitrogen containing gas-phase negative ions e.g. CN^-, C_3N^-/C_4H^-, and C_5N^- (Vuitton et al. 2009; Desai et al. 2017b), corresponding to mass groups 1–3 shown in Fig. 2. Further ion-neutral chemistry involving reactions such as proton transfer results in the growth of positive, negative, and neutral particles up to a few 100u (Vuitton et al. 2009, 2019; Žabka et al. 2012; Dobrijevic et al. 2016), some of which are sub-nm size aerosol embryos (Lavvas et al. 2013). The neutral aerosols react predominately with free electrons due to their higher mobility. This reduces the electron populations and produces higher mass negatively charged aerosols, which in turn continue to grow larger mainly by recombining with positive ions but also by coagulating with other aerosols. Lavvas et al. (2013) investigated these processes in detail and show that masses in the ELS spectra <100u are gas-phase negative ions, corresponding to mass groups 1–5 in Fig. 2, whereas the higher masses (groups 6 and 7) are negatively charged aerosols.

Most of the mass groups in Fig. 2 show peaks at or near the centre of their respective mass ranges. The mass group boundaries are based on these recurring peaks which are also observed during other fly-bys. The only mass group that does not appear to have a distinct peak is group 5. Spectra from many other fly-bys (not shown) do show a peak in mass group 5. Therefore, the species making up mass group 5 could be different to those observed during other fly-bys, or they are simply not as abundant. The other groups' agreement on the approximate peak locations may indicate that some species are the same as those commonly observed. The peaks of groups 6 and 7 generally tend to be much broader peaks than the other mass groups. The maximum of mass group 6 appears to remain at the same mass, whereas the mass group 7 maximum moves to higher masses at lower altitudes. We also note that due to the logarithmically spaced energy per charge bins (and hence mass bins), the mass bin size at higher masses is much larger than at lower masses. We may therefore not be able to see some structure and possibly more peaks within the higher mass groups. The growth of the negatively charged aerosols is discussed in detail by Lavvas et al. (2013). We can see from Fig. 3(b) that mass group 7 is almost always present at altitudes below 1000 km, but only some data points are above 625 u/q (the lower mass group 7 boundary) at altitudes >1000 km. The general behaviour and evolution of the mass groups is consistent with the shift in the simulated distributions described by Lavvas et al. (2013, fig. 4A).

If we take note of the energy range of each spike-shaped negative ion signature in the spectrogram (Fig. 1), and the altitude at which they are observed from the bottom panel, we can see that the altitude trend observed in Figs 3(a) and (b) is also evident during individual fly-bys such as T16. The longer structures (i.e. larger energy and hence mass range) are observed at the lowest altitudes, whereas at higher altitudes only short structures (i.e. low-mass only) are present. This is also apparent in the spectra shown in Fig. 2. Wellbrock et al. (2013) report that the lower mass group densities tend to peak at slightly higher altitudes than the heavier ions (also see Section 1). The spectra in Fig. 2 show counts s^{-1}, which is proportional to number density (not shown). Therefore, this trend can also be observed in the T16 data.

Converting the instrument specific units of processed negative ion counts s^{-1} to number density can be achieved by assuming that the count rate multiplied by the ion charge represents a current of ions in the ram direction, as described in more detail by Wellbrock et al. (2013). The main issue with this conversion is that it involves the MCP efficiency which is not well characterized for negative ion measurements; CAPS-ELS was designed and calibrated to measure electrons. Large uncertainties are therefore associated with number density calculations. Wellbrock et al. (2013) and other previous studies used an MCP efficiency of 5 per cent based on studies by Fraser (2002) to calculate number densities. They also describe the limitations associated with using absolute values and

comparing relative number densities. Studies by Peko & Stephen (2000) suggest that an MCP efficiency closer to 25 per cent may be more accurate. A recent investigation by Fontanese et al. (2018) also indicates that values may be higher than 5 per cent, and may even reach 100 per cent in some cases. Using a higher efficiency in the conversion results in lower density values. The peak total negative ion density measured during T16 using a 5 per cent MCP efficiency is 249 cm^{-3}, which may be closer to the upper bound of the density uncertainty. MCP efficiencies of 25 per cent and 50 per cent correspond to total T16 negative ion peak densities of 50 and 25 cm^{-3}, respectively.

The T16 density of 249 cm^{-3} is average compared to peak total negative ion densities measured by CAPS-ELS during other Titan fly-bys analysed by Wellbrock et al. (2013) and using the same MCP efficiency of 5 per cent. T16 densities are therefore not unusually high; it is only the recorded highest masses during T16 that are particularly high. We note that the MCP efficiency is associated with a systematic uncertainty only; therefore, using a different efficiency (consistently applied to all fly-by data) would not change any relative density trends. Similarly, the T16 number densities of individual mass groups (not shown) are also average compared to other fly-bys. Unsurprisingly, the only exception is the highest mass group (mass group 7: 625 u/q and above): Using a 5 per cent MCP efficiency, the peak density is 159 cm^{-3}, which is moderately high compared to other fly-bys (cf. Wellbrock et al. 2013, fig. 2). An important point to note here is that this may (at least in part) be due to simply a larger range of negative ion species being covered by this mass group range; only a handful of fly-bys reach negative ion masses that exceed 2000 u/q; therefore, mass group 7 covers a much smaller range of masses (and hence species) for most fly-bys.

We now consider why the T16 masses were significantly higher than other fly-bys. The three highest mass data points in Fig. 3(e) were all observed during T16 and there is some indication that the very highest masses are observed at high northern latitudes. However, if we consider polar fly-bys only, observations at later times during the Cassini mission indicate considerably lower maximum masses as shown in Table 1. T16, T32, and T64 were all low altitude fly-bys and therefore there was no altitude bias; T65 is also shown for completeness however note that the CA altitude was higher. All four fly-bys were in a similar SZA range; hence, this is also unlikely to cause any SZA bias. It was northern winter solstice in the Saturn system in 2002, followed by equinox in 2009. T16 was therefore the polar fly-by closest in time to the northern winter solstice. It is possible that the highest masses (greater than 10 000 u/q) observed during T16 are a direct result of a combination of polar and seasonal effects. Long-term exposure to limited polar winter conditions and a resulting limited solar flux could allow ions to grow without high destruction rates due to photochemical reactions such as photodetachment. The photodetachment rate depends on particle size and charge, and also the solar flux at different altitudes. Photodetachment cross-sections have been studied for some carbon chain anions (e.g. Best et al. 2011; Douguet, Kokoouline & Orel 2014) but not for the aerosol embryo anions in the specific conditions at Titan. However, we do know that the efficiency of photodetachment increases with increasing ion size (Lavvas et al. 2013), making the high masses such as those observed during T16 particularly vulnerable; it may be impossible for them to survive in any other conditions where solar flux is not as restricted over longer periods of time.

Fig. 3(e) also shows some medium to high masses (mid-1000s of u/q) at mid-latitudes. The controlling factors responsible are not as clear for these data points. Fig. 3(c) suggests that one contributing factor could be the night side; however not all nightside fly-bys exhibit such moderately high masses, indicating that there are also other contributing controlling factors.

It is not clear what controlling factor is responsible for the higher-than-average mass data points at specific altitudes in 2007 (orange) and 2008 (green) in Figs 3(a) and (b). Fig. 3(e) shows that sampling in 2007 was mostly in the Northern hemisphere, suggesting again a possible seasonal (winter) effect. Solar activity was not very variable due to the long solar minimum of solar cycle 23/24 during the years sampled. The solar radio F10.7cm flux at 1 au remained low until 2010 when it started to increase slightly (see e.g. fig. 1 in Westlake et al. 2014). The absence of any higher masses in 2012 (which was well into the rising phase of solar cycle 24) suggests that high masses have some preference for low solar activity; however, other controlling factors could also be responsible. Westlake et al. (2014) report that higher methane concentrations were observed during solar minimum compared to solar maximum. This is believed to be due to higher photochemical reaction rates during solar maximum, which in turn create more C_2 hydrocarbon building blocks leading to the production of more of the more complex hydrocarbon chains. However, fewer photodestruction reactions due to solar minimum may provide better conditions for the negative ions to grow to higher masses at a specific altitude. Shebanits et al. (2017) investigated the effects of changing EUV fluxes on positive and negative ion charge carriers using RPWS-LP and found that dayside charge densities increased by a factor of 2 from solar minimum to maximum, whereas nightside densities decreased.

There were no more low altitude polar fly-bys during the Cassini mission after those listed in Table 1 to test the theory that polar winter conditions result in the highest negative ion masses. The T116 fly-by took place at the right time to see if the polar winter in the Southern hemisphere yielded similar results; however, the CA altitude was too high (1400 km) and CAPS was also turned off. Future missions to Titan are therefore needed to confirm that polar winter conditions create the right conditions for negative ions to grow to the highest masses. Future studies may also investigate if there is a link to seasonal changes at the poles at lower altitudes (e.g. Teanby et al. 2008; Coustenis et al. 2018; Larson 2019; and references therein).

5 SUMMARY AND CONCLUSIONS

We presented a detailed study of negative ions observed during the Cassini polar Titan fly-by T16 using CAPS-ELS. We discussed the evolution of mass spectra at different altitudes. The highest masses are observed at the lowest altitudes sampled, a trend which is evident in data from other fly-bys too. We also observed that the peak of group 7 (the heaviest mass group, 625+u/q) in the mass spectra moves to higher masses at lower altitudes, which agrees with modelling results by Lavvas et al. (2013). Using a larger data set, we also extended the Coates et al. (2009) study in order to investigate what conditions are required for the highest negative ion masses to form, including seasonal effects. Masses observed in 2007 and 2008 appear to be higher than the average at a specific altitude; the reason for this is unclear but may be related to a solar cycle effect. We focused on why the ion masses observed during T16 were significantly higher than any other fly-by. When comparing T16 to other polar fly-bys, it became apparent that the T16 masses are especially high as a result of not only a latitudinal effect but also a seasonal effect. Despite a limited number of samples available, we suggest that the best explanation based on the data available is related to the combination of polar and seasonal (winter)

conditions, which provide an environment in which the solar flux is restricted over long periods of time. We propose that it is the long-term restriction of photochemical destruction reactions such as photodetachment, whose efficiency increases with increasing ion mass, that allows the ions to grow to masses exceeding 10 000 u/q. Our results may also be important in the growth of high-mass anions in other atmospheres where photochemical reactions involving nitrogen and methane are present, such as Pluto, Charon, Triton, and some extrasolar planets and moons.

ACKNOWLEDGEMENTS

We thank the CAPS team for useful discussions and L. Gilbert and Gethyn R. Lewis for software support. We acknowledge the support of CAPS-ELS science by STFC (grant ST/S000240/1) and of the CAPS-ELS operations and software team by ESA via the UK Space Agency. Work in the USA was supported by NASA JPL contracts 1243218 and 1405851 to the Southwest Research Institute. This work has benefited from discussions within International Space Science Institute (ISSI) International Team 437.

REFERENCES

Ågren K., Edberg N. J. T., Wahlund J. E., 2012, Geophys. Res. Lett., 39, L10201
Ali A., Sittler E. C., Chornay D., Rowe B. R., Puzzarini C., 2015, Planet. Space Sci., 109, 46
Backes H. et al., 2005, Science, 308, 992
Best T. et al., 2011, ApJ, 742, 63
Broadfoot A. L. et al., 1989, Science, 246, 1459
Brown R. H., Lebreton J. P., Waite J. H., 2010, Titan from Cassini-Huygens, Springer Monograph Book, preprint (arXiv:1011.1669v3)
Chaizy P. et al., 1991, Nature, 349, 393
Coates A. J., Crary F. J., Lewis G. R., Young D. T., Waite J. H., Sittler J. C., 2007, Geophys. Res. Lett., 34,
Coates A. J., Wellbrock A., Lewis G. R., Jones G. H., Young D. T., Crary F. J., Waite J. H., 2009, Planet. Space Sci., 57, 1866
Coates A. J. et al., 2010a, Faraday Discussions, 147, 293
Coates A. J. et al., 2010b, Icarus, 206, 618
Cordiner M. A., Buckle J. V., Wirström E. S., Olofsson A. O. H., Charnley S. B., 2013, ApJ, 770, 48
Coustenis A., Jennings D. E., Achterberg R. K., Bampasidis G., Nixon C. A., Lavvas P., Cottini V., Flasar F. M., 2018, ApJ, 854 , L30
Cui J., Yelle R. V., Volk K., 2008, JGRE, 113, E10004
Desai R. T., Cowee M. M., Wei H., Fu X., Gary S. P., Volwerk M., Coates A. J., 2017a, J. Geophys. Res.: Space Phys., 122, 10,408
Desai R. T. et al., 2017b, ApJ, 844, L18
Desai R. T. et al., 2018, Geophys. Res. Lett., 45, 1704
Dobrijevic M., Loison J. C., Hickson K. M., Gronoff G., 2016, Icarus, 268, 313
Douguet N., Kokoouline V., Orel A. E., 2014, Phys. Rev. A, 90, 063410
Dubois D., Carrasco N., Bourgalais J., Vettier L., Desai R. T., Wellbrock A., Coates A. J., 2019, ApJL, 872, 31
Fontanese J., Clark G., Horanyi M., James D., Sternovsky Z., 2018, J. Geophys. Res.: Space Phys., 123, 9936
Fraser G., 2002, Int. J. Mass Spectrom., 215, 13
Gladstone G. R. et al., 2016, Science, 351, aad8866
Grundy W. M. et al., 2016, Nature, 539, 65
Gurnett D. A. et al., 2004, Space Sci. Rev., 114, 395
Hargreaves J. K., 1992, The Solar-terrestrial Environment: An Introduction to Geospace – The Science of the Terrestrial Upper Atmosphere, Ionosphere and Magnetosphere, Cambridge University Press, Cambridge.
Hörst S. M., 2017, JGR-Planets, 122, 432
Jones G. H. et al., 2009, Geophys. Res. Lett., 36, L16204
Larson E. J. L., 2019, ApJ, 872, L23
Lavvas P. et al., 2013, Proc. Natl. Acad. Sci., 110, 2729
Lindgren E. B., Stamm B., Chan H. K., Maday Y., Stace A. J., Besley E., 2017, Icarus, 291, 245
Michael M., Tripathi S. N., Arya P., Coates A., Wellbrock A., Young D. T., 2011, Planet. Space Sci., 59, 880
Millar T. J., Walsh C., Field T. A., 2017, Chem. Rev., 117, 1765
Mukundan V., Bhardwaj A., 2018, ApJ, 856, 168
Nixon C. A. et al., 2018, Planet. Space Sci., 155, 50
Peko B. L., Stephen T. M., 2000, NIMPB, 171, 597
Shebanits O., Wahlund J.-E., Mandt K., Ågren K., Edberg N. J. T., Waite J. H., 2013, Planet. Space Sci., 84, 153
Shebanits O. et al., 2016, JGRA, 121, 10,075
Shebanits O., Vigren E., Wahlund J.-E., Holmberg M. K. G., Morooka M., Edberg N. J. T., Mandt K. E., Waite J. H., 2017, JGRA, 122, 7491
Teanby N. A. et al., 2008, Icarus, 193, 595
Teolis B. D. et al., 2010, Science, 330, 1813
Volwerk M., Kivelson M. G., Khurana K. K., 2001, J. Geophys. Res. Space Phys., 106, 26033
Vuitton V., Lavvas P., Yelle R. V., Galand M., Wellbrock A., Lewis G. R., Coates A. J., Wahlund J.-E., 2009, Planet. Space Sci., 57, 1558
Vuitton V., Yelle R. V., Klippenstein S. J., Hörst S. M., Lavvas P., 2019, Icarus, 324, 120
Waite J. H. et al., 2005, Science, 308, 982
Waite J. H., Young D. T., Cravens T. E., Coates A. J., Crary F. J., Magee B., Westlake J., 2007, Science, 316, 870
Wei H. Y., Russell C. T., Dougherty M. K., Neubauer F. M., Ma Y. J., 2010, JGRE, 115, E10007
Wellbrock A., Coates A. J., Jones G. H., Lewis G. R., Waite J. H., 2013, Geophys. Res. Lett., 40, 4481
Westlake J. H., Waite J. H., Bell J. M., Perryman R., 2014, JGRA, 119, 8586
Young D. T. et al., 2004, Space Sci. Rev., 114, 1
Žabka J., Romanzin C., Alcaraz C., Polášek M., 2012, Icarus, 219, 161

APPENDIX: LIST OF FLYBYS

The table below shows a list of all Cassini Titan fly-bys with observed negative ion signatures that were used in this study. DOY – Day of Year; SLT – Saturn Local Time; TLT – Titan Local Time; Solar Zenith Angle – SZA. Each '(yes)' in the 'in shadow' column means that part of the fly-by where negative ions were observed was in shadow (extended version of table from Coates et al. 2009 and Wellbrock et al. 2013). The altitude columns shows the altitude at which the centre of the lowest negative ion signature was observed; this is usually very close to the CA altitude.

Table A1. Titan fly-bys

Fly-by	Date	UT (hh:mm:ss)	DOY	Altitude (km)	SLT (hh:mm:ss)	TLT (hh:mm:ss)	Latitude (°N)	SZA (°)	In shadow?
T16	22-Jul-06	00:24:58	203	954	02:26:42	18:29:17	87.8	106.7	No
T17	07-Sep-06	20:17:33	250	1000	02:19:47	10:44:30	21.7	41.8	No
T18	23-Sep-06	18:58:54	266	960	02:17:03	14:23:49	70.5	89.6	No
T19	09-Oct-06	17:30:00	282	980	02:14:13	14:14:34	61.4	81.3	No
T20	25-Oct-06	15:57:15	298	1042	02:11:40	10:52:39	8.6	29	No
T21	12-Dec-06	11:40:05	346	1002	02:02:51	20:52:30	49.4	128.4	No
T23	13-Jan-07	08:38:03	13	1004	01:57:26	13:53:46	33	54.3	No
T25	22-Feb-07	03:11:57	53	1003	13:51:21	00:30:38	27.9	163.9	(Yes)
T26	10-Mar-07	01:47:27	69	981	13:48:38	01:25:32	23.6	157.3	(Yes)
T27	26-Mar-07	00:23:50	85	1013	13:46:03	01:49:46	42.9	141.9	(Yes)
T28	10-Apr-07	22:56:51	100	992	13:43:23	01:21:14	44.1	144.2	(Yes)
T29	26-Apr-07	21:31:34	116	983	13:40:47	01:10:22	51.9	138.2	(Yes)
T30	12-May-07	20:08:54	132	961	13:38:21	01:06:30	62.8	128.1	(Yes)
T32	13-Jun-07	17:46:52	164	965	13:35:00	04:35:48	87.2	102.9	No
T36	02-Oct-07	04:41:57	275	973	11:29:25	16:45:54	− 59.2	71.8	No
T39	20-Dec-07	22:58:08	354	970	11:21:52	11:24:47	− 69.1	60.4	No
T40	05-Jan-08	21:30:30	5	1015	11:19:41	14:28:17	− 11.1	36.6	No
T41	22-Feb-08	17:32:37	53	1003	11:13:04	12:48:37	− 33.2	27.6	No
T42	25-Mar-08	14:27:15	85	1001	11:07:07	12:49:10	− 28.9	24.3	No
T43	12-May-08	10:01:52	133	1002	10:59:11	13:46:27	17.8	36	No
T46	02-Nov-08	17:38:11	308	1109	10:28:14	00:37:34	5.3	170.6	Yes
T48	05-Dec-08	14:25:36	340	961	10:22:18	10:25:44	−11	24.5	No
T49	21-Dec-08	12:59:16	356	972	10:19:24	06:36:19	− 47.5	81.3	No
T50	07-Feb-09	08:50:52	38	967	10:12:33	01:42:58	− 33.8	136.2	(Yes)
T55	21-May-09	21:26:08	141	966	21:57:06	22:00:27	− 19.1	144.4	(Yes)
T56	06-Jun-09	19:59:12	157	968	21:54:40	22:00:57	−28	139.5	(Yes)
T57	22-Jun-09	18:31:10	173	955	21:52:10	22:07:31	− 34.9	135.8	(Yes)
T58	08-Jul-09	17:02:35	189	966	21:49:38	22:07:42	− 44.7	128.5	(Yes)
T59	24-Jul-09	15:32:35	205	957	21:47:00	22:08:20	− 54.7	120.6	No
T61	25-Aug-09	12:50:29	237	961	21:42:18	18:09:34	−18	92.4	No
T64	28-Dec-09	00:16:51	362	952	16:57:49	17:19:36	82.7	86.5	No
T65	12-Jan-10	23:10:35	12	1074	16:56:39	04:38:16	− 82.2	95.2	No
T71	07-Jul-10	00:22:35	188	1004	16:03:36	07:22:56	− 56.3	83	No
T83	22-May-12	01:09:51	143	957	13:44:24	17:18:07	73	73.1	No

This paper has been typeset from a TEX/LATEX file prepared by the author.